Journal Name

ARTICLE TYPE

Cite this: DOI: 00.0000/xxxxxxxxxx

Visualisation of Aromaticity and Antiaromaticity via the Computation of the Chemical Shielding on Multi-Dimensional Grids

Dylan Morgan[a]

Received Date
Accepted Date

DOI: 00.0000/xxxxxxxxxx

Visualising and quantification of aromaticity in molecular structures effectively is of high importance and necessity for publications in chemistry. Despite this importance, the computational toolbox for doing so is quite limited, where many of the methods used are either outdated and inflexible, or necessitate substantial expertise to use and interpret effectively. Nucleus-independent chemical shift (NICS) has continuously presented itself as effective and flexible for visualisation of the associated isotropic magnetic shielding (IMS). Presented here are a set of open-source python scripts denoted as IMS-plot, for generation of 1D graphs and 2D contour plots to enable clear visualisation of (anti)aromatic regions, which are based off of the now widely used NICS method. Usage of IMS-plot is demonstrated against benzene, several PAHs, larger, complex macrocycles, and in some instances, for triplet excitation states and non-neutral species. IMS-plot is shown to be a powerful tool for reliably predicting regions of (anti)aromaticity, local and global aromaticity, and molecular aromatic switching, even when Hückel's and Baird's rules' fail.

Introduction

Aromaticity is an inherently challenging phenomenon to quantify, which has puzzled chemists for over 150 years.[1] It has even been difficult to settle on a rigid definition for the matter, with Hückel, Pauling, Baird, and Clar all being some notable examples of individuals who have contributed significant advancements to the subject.[2–5] The importance of this cannot be understated, with aromatic systems featuring so prevalently across all fields in chemistry. Whilst frustrating, the difficulty is understandable, after all, how does one quantify a quantum phenomena like the level of delocalisation of electrons around a molecule?

Fortunately, the late Paul Von Schleyer, who in and of himself had already made some marked contributions to post-Hückel aromaticity theory, also developed a criterion for quantifying aromaticity based on the influence of aromaticity on the chemical shift of other species.[6–8] As every undergraduate chemist is aware, the chemical shift of a hydrogen environment in an aromatic system is deshielded when compared to its non-aromatic counterpart upon measurement by NMR. Contrasting this, antiaromatic compounds, which are physically manifested as systems on the verge of losing their aromaticity, experience increased shielding around hydrogen environments when compared to similar non-aromatic compounds. Nucleus-Independent Chemical Shift (NICS), as Von Schleyer describes the method, utilises this concept for quantification of aromaticity by calculating the chemical shift at a point in space where there is no atom.[9,10] As will be discussed later, this point is far from arbitrary.

Ring currents are the phenomenon which are responsible for shielding or deshielding species in an aromatic or antiaromatic system. An applied magnetic field will instigate a flow of the delocalised, conjugated electrons in an aromatic compound like benzene, perpendicular to the direction of the applied field. The effect of this can be seen in **figure 1**. This in turn, creates its own induced magnetic field that can either oppose or enhance that of the original field. In aromatic systems, the ring current is clockwise, or diatropic, and opposes the applied field, causing deshielding of chemical species outside the ring. In antiaromatic rings, the ring current is anticlockwise, or paratropic, and enhances the applied field, causing increased shielding of chemical species outside the ring. The physical realisation of this becomes apparent when performing NMR spectroscopy experiments. Essentially, NICS models this effect via calculation of the isotropic magnetic shielding (IMS) value to be able to differentiate between aromatic and antiaromatic cycles.

To calculate NICS for an aromatic compound, ghost atoms (also known as dummy atoms or Bqs), are used as a reference point to calculate this value, which operate on the basis of, and can be specified using Cartesian coordinates. The quantum chemistry program Gaussian enables use of this feature, and a full description can be found on the Gaussian manual.[12,13] Essentially, they have no nuclear charge or electrons, but are otherwise treated the same as other atoms by Gaussian. Therefore they do not influence the chemistry of any other atom. The IMS of the ghost atom is calculated, and the result multiplied by -1 to fit with the widely-

[a] *Department of Chemistry, Loughborough University, Loughborough, Leicestershire, LE11 3TU. E-mail: d.morgan-16@student.lboro.ac.uk*

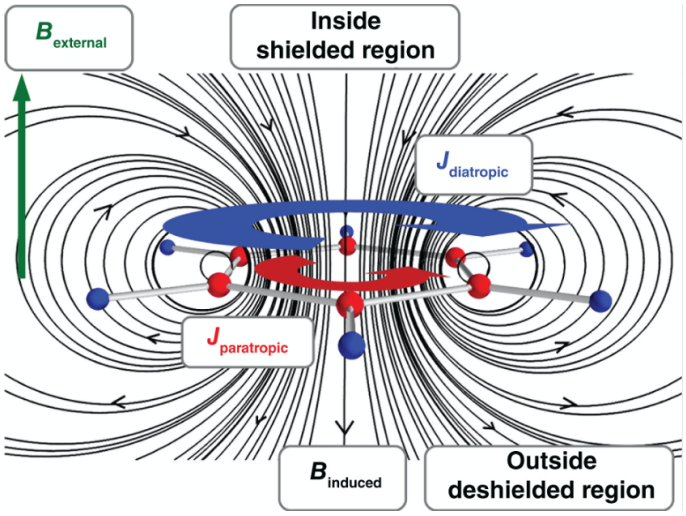

Fig. 1 Diagram showing the different ring currents using benzene as an example. The diatropic ring current ($J_{\text{diatropic}}$, *blue*) forms outside the ring and induces a magnetic field (B_{induced}, *black*) opposing the applied magnetic field (B_{external}, *green*), causing deshielding of components outside the ring. If benzene were hypothetically antiaromatic, the ring current would be paratropic ($J_{\text{paratropic}}$, *red*), B_{induced} would align with and enhance B_{external}, and cause species situated outside the ring to have increased shielding. Image courtesy of Sundholm et al.[11]

recognised NMR convention. This inverse of the calculated IMS value can therefore be considered a chemical shift of a theoretical species at the location of the ghost atom. Therefore, positive values represent additional shielding and antiaromatic behaviour, whereas negative values indicate deshielding and aromaticity. If NICS is calculated as ∼0 ppm, then the structure is non-aromatic.

Initially, it was proposed that NICS should be calculated from the centre and in the plane of a ring (NICS(0)), which could be determined from the non-weighted average of all atoms in the ring. It was determined that NICS(0) was heavily affected by the σ orbital contributions, but could be avoided by placing the ghost atom 1 Å above the plane - NICS(1).[14–16]

The idea behind the work being presented here is to utilise this concept of calculating NICS at a given point, except across an entire 1D or 2D array (line or surface). Whilst there are limited instances of IMS plots that have been used in research already, it is not a trivial task, and computations of this nature are far from routine.[17–21] However, there has yet to be a formalised approach or code that has been made available for general use to easily generate these plots. 1D arrays were first used by Amnon Stanger[17] to probe the z-plane of planar molecules, and to divide NICS into the in- and out-of-plane contributions, which revealed certain problems with NICS(0) and NICS(1) for quantification in specific instances. The aim of running benzene in 1D was to prove that we could achieve reproducible results consistent with those reported by Stanger, and that the development of the method thus far was producing reliable data before moving on to developing the technique further.

Furthermore, 2D and even 3D plots have also been seen in publications in recent years - no doubt as computations with large NICS arrays have become more tractable for modern computers. Notably, theoretical calculations by Karadakov[21] have ended the debate on the nature of aromaticity in norcorrole and Ni norcorrole, where prior to his paper, the general consensus was that they were antiaromatic.[22–24] Karadakov's research has shown through a visualisation based method of creating 3D IMS plots that this is not the case, and in fact the central structure is antiaromatic, but "surrounded by an aromatic 'halo'".[21]

It is the purpose of this work to rectify this problem and develop a computational tool for use by chemists in all fields to assist in their research. As the process can involve addition of a large number of dummy atoms to input files, and hundreds of input files, it becomes impractical to perform this task manually. By automating this using commonly used command line-based tools, written in python, and making the source code publicly available, it aims to become a practical tool for use, not just by computational chemists, but with minimal training, practical chemists too for use in their publications.

One example of such a molecule is [2.2.2.2]paracyclophane-1,9,17,25-tetraene (PCT), which was found in 2020 by Eder et al.[25] to be an excellent and stable organic material for use as an electrode in sodium ion batteries. The structure of PCT consists of 4 phenylene groups connected by 4 vinylenes to form a macrocycle, where each of the phenylene rings are aromatic. One feature of PCT that makes it slightly unusual - especially for an electrode, is that upon reduction to its dianion, PCT^{2-}, it has been found to switch its aromaticity from the 4 local phenylene rings, to globally across the whole macrocycle. Using this method of creating an IMS plot presented here, we can clearly understand and visualise the aromatic pathways of PCT and PCT^{2-} through quantitative calculations.

Thus, this work is structured as follows: firstly, the particulars of the method used, the code written, and the computational details will be addressed. Then, the results of the computations and the generated IMS plots will be shown and discussed in detail in the context of physical chemistry. Finally, we will analyse what conclusions can be drawn from the results, detail suggestions for future work and research, and acknowledge some of the shortcomings of this work.

To demonstrate the effectiveness of this method, five independent molecules were selected to be optimised and for calculation and plotting of their isotropic NICS values. As the 1D Bq array as used by Stanger[17] was first used more than 15 years ago, only benzene was run in 1D to show reproducibility with these results. Here, we will also present and compare these with the benzene T_1 state. IMS plots were then created for the following: singlet and triplet anthracene, singlet and triplet biphenylene, norcorrole (H_2Nc), nickel norcorrole (NiNc), PCT, and its reduced form; PCT^{2-}. Where possible, the IMS plots were created from NICS(1), and was used to assess the nature of aromaticity of the molecules described above. However, it was anticipated that PCT would be non-planar as it has been reported that each each benzene ring was locally aromatic, and that PCT^{2-} would be planar as this has been reported to be globally aromatic.[25] Similarly, both NiNc and H_2Nc have been reported to be non-planar, with both being bowl-shaped, whilst a twisted conformer also exists for PCT^{2-}.[21] In the computations we performed, only the bowl-

shaped conformer was used for H_2Nc.

Methods

Python scripts were written to automate the process of adding ghost atoms or dummy atoms (Bqs) and plotting graphs of them against their isotropic NICS values. These scripts were collated into a set of tools called IMS-plot, which can be downloaded from this Github repository as open source code.[26] Note that this repository is still in active development, and is likely to change regularly in future as features are added and improvements are made.

Firstly, benzene and anthracene were drawn in the molecular visualisation program JMol,[27] and pre-optimised using the built-in force field functions. This provided an adequate starting point for the structures of anthracene and benzene to continue with the DFT calculations. A geometry optimisation was then performed in Gaussian09. The importance of obtaining an accurate structure of the molecule notwithstanding, this step is necessary as in the act of optimising the geometry, Gaussian09 also centres the atomic coordinates of the molecule around the origin of the grid. The necessity of this will be discussed later.

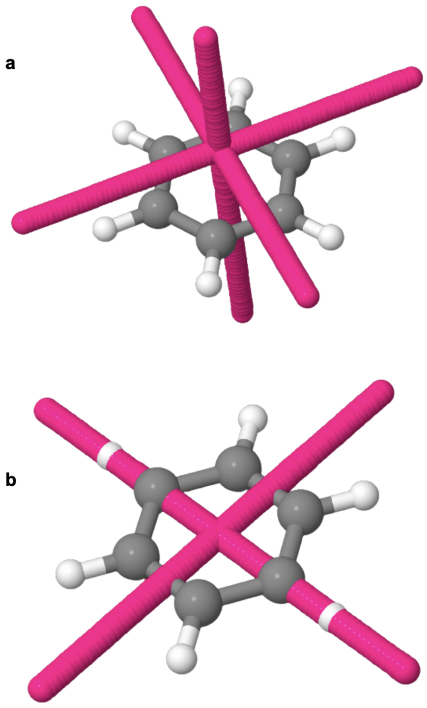

Fig. 2 The spatial locations of the out-of-plane and through-plane (**a**), and in-plane (**b**) Bq 1D arrays used for benzene to generate the plots in **figures 4 - 6**

Once the optimisations had completed, Open Babel[28] was employed to parse the optimised coordinates from the output file to generate a new input file. Then, a 1D array of Bqs was generated and appended to the new input file using the 1D ghost atom generator script (1d_gen.py) from IMS-plot. They were added 1 Å above the plane of the molecule, and in the plane in both the x and y directions, and through the C_6 symmetry element for benzene in the z direction to separate files. In the instance of

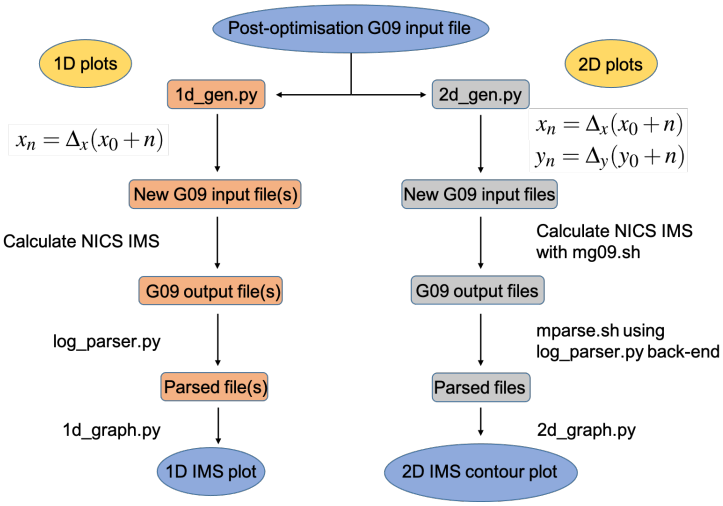

Fig. 3 Flowchart for generation of IMS plots from post-optimisation of the structure using IMS-plot scripts. The equations refer to the back-end for ghost atom generation, where x_n and y_n are the x- and y-coordinates, Δ_x and Δ_y are the vector spacings, x_0 and y_0 are the start points for the arrays, and n refers to the nth ghost atom.

benzene, Bqs were generated between -4 to +4 Å from the origin of the molecule, spaced 0.1 Å apart. The out-of-plane arrays are depicted in **figure 2a**, whilst the in-plane arrays are in **figure 2b**. For all 1D computations, these vector spacings were used. Had the molecule not been centred around the origin of the coordinate grid beforehand, it would not have been possible to specify the exact, desired directions and locations of the arrays. For both 1D and 2D scripts, the non-weighted average does not need to be taken for all other atoms, as Lampkin et al.[19] have explained.

The Gaussian09 'nmr' command enables "prediction of [the] NMR shielding tensors and magnetic susceptibilities using the Hartree-Fock method, all DFT methods and the MP2 method".[29] Thus, this calculation was performed for the 5 different arrays of Bqs. The NICS isotropic values, magnetic shielding tensors, and Bq coordinates were parsed from the Gaussian output file using the log parser script (log_parser.py). Finally, graphs of isotropic NICS values were plotted as a function of the distance from the origin of the coordinate grid using the 1D graph plotter script (1d_graph.py), which utilises the matplotlib.pyplot python library. This method was repeated for both the singlet and triplet states of benzene. Finally, before plotting the data, all the isotropic values for each dummy atom were converted to the more meaningful and widely used chemical shift metric in ppm. For visualisation of the physical molecular structures, JMol was used.

To create a 2D visualisation of a molecule, the process is much the same as described above for the 1D graph, with minor changes to some of the maths involved. However, due to the massive number of Bqs which were being generated and appended to the input file, Gaussian was not able to calculate the isotropic NICS values, and the job would invariably terminate with an error. Upon investigation into this, it was found that the maximum number of Bqs Gaussian09 could consistently and successfully run from an input file was approximately 25. The 2D generator script (2d_gen.py)

was used to create the a 2D array of ghost atoms, whilst also creating the appropriate number of files in such a way that each file would have a maximum of 25 ghost atoms. As this can generate hundreds of files for larger molecules - especially when close vector spacings are used, a bash script was written to automate running multiple Gaussian input files serially (mg09.sh). Another bash script (mparse.sh) was also written to automate parsing the data from multiple output files. The matplotlib.pyplot.contourf function was then used in the 2d_graph.py script to create a filled contour plot from 3 x 1D arrays to visualise the results, also called an IMS plot. Finally, structures of the molecules obtained from JMol were overlaid onto the IMS plots to be able to more easily identify which features of a chemical structure could be attributed to its NICS contributions. A flowchart of this process can be found in **figure 3**, which also explains some of the back-end behind generation of the ghost atom arrays.

An additional challenge is presented when creating IMS plots of the non-planar molecules. In the case of H_2Nc and NiNc, both arrays of Bqs were taken 1 Å above the centre of the macrocylce. Further calculations of NICS were also run in additional planes for both norcorrole derivatives, to further illuminate their aromatic/antiaromatic features, NICS values were also calculated in the yz-plane.

In the case of PCT, NICS was calculated for multiple 2D arrays that were drawn from the centre of the of the molecule (and completely bisecting it), to 2 Å above this point, at 1 Å intervals. Anthracene was primarily used here as a tractable, but nonetheless compelling molecule to assess the efficacy of the developed 2D method. NICS investigations on anthracene were performed 1 Å above the plane in the singlet state with 0.2 Å vector spacings, with shorter 0.1 Å vector spacings, in the triplet state, and in the plane. Finally, IMS plots were also generated for biphenylene to demonstrate and examine how the technique performs on smaller rings, and visually differentiate aromatic-switching between the T_1 excitation and S_0 ground states. Again, the aromatic nature of biphenylene is already well documented, importantly with regard to its ability to switch its aromaticity, so it provides an excellent example of a species that we can compare the antiaromatic visualisation capabilities of our method against.[30]

Computational Details

The geometry optimisations and calculations of NICS values were performed using the PBE0/def2-SVP functional and basis set, with 12 CPU cores operating in parallel and 16 GB of RAM on the Gaussian09 quantum chemistry program. This was achieved using the Sci-Grid high-performance computing (HPC) cluster at Loughborough University.

PBE0 is a hybrid functional which takes 25% of the contributions for the exchange energy from Hartree-Fock, the rest from the GGA functional PBE, and all of the correlation energy from PBE.[31–34] The PBE0 functional was used with the def2-SVP basis set, which uses two basis functions to calculate the wavefunctions for the valence orbitals, the precedence for which is that the valence orbitals are usually the ones to participate in bonding, so are more important to be accurately accounted for, whilst still maintaining tractability and reasonable calculation times. Furthermore, this basis set also has additional functions to include polarizability of orbitals.[35,36] The 'def2', or default 2, is a more modern approach to this basis set which solves some of the issues with earlier versions of this basis set.[37,38] It was decided that PBE0/def2-SVP would be appropriate for these computations as it is accurate enough to visualise aromaticity and correctly calculate NICS isotropic values, but anything more expensive - such as TZVP for instance, would not significantly improve the accuracy and quality of the results. This also allowed for more calculations in the time frame available, whilst still demonstrating the efficacy of this method, and not hindering other users of the HPC cluster by occupying nodes and computational power unnecessarily.

Results and Discussion

The IMS plots generated are able to show regions of both aromaticity and antiaromaticity in the molecules discussed here, where, by default, aromatic regions are orange or red in colour (negative values), and antiaromatic regions are blue (positive values). The isotropic NICS values for each ghost atom were converted to chemical shift, δ, and are portrayed as such in the IMS plots. Lighter colours represent areas that have little or no (anti)aromatic character, and the converse applies to darker areas.

Benzene

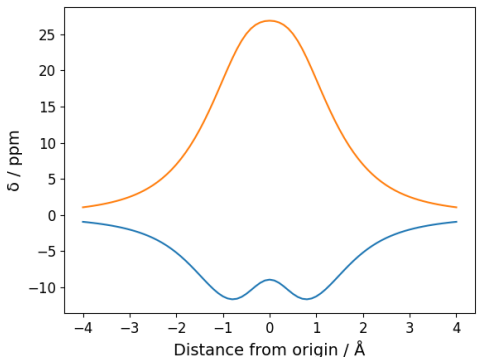

Fig. 4 Isotropically averaged chemical shift of benzene in the ground S_0 state (*blue*) and the T_1 triplet excited state (*orange*) as a function of distance away from the non-weighted mean average of the atoms in benzene (referred to here as the origin). Arrays were placed through the benzene C_6 symmetry element (also shown in **figure 2**). Results were obtained using the PBE0/def2-SVP functional and basis set.

The 1D calculations of benzene are shown in **figures 4 - 6**. In **figure 4**, a chemical shift of roughly -10 ppm just under 1 Å above and below the ring can be observed, with a slight decrease in δ just under 1 Å either side of the origin. The negative δ expectedly shows aromaticity. Here we have shown to have successfully replicated Stanger's findings.[17] We can also report the antiaromatic T_1 benzene species with a peak δ of 25 ppm at the centre of the ring and 17 ppm at NICS(1).

In **figure 5**, we can observe the chemical shift from a 1D array of ghost atoms placed such that the ghost atoms bisect the bonds between carbons. **Figure 6** is similar to this, but directly above

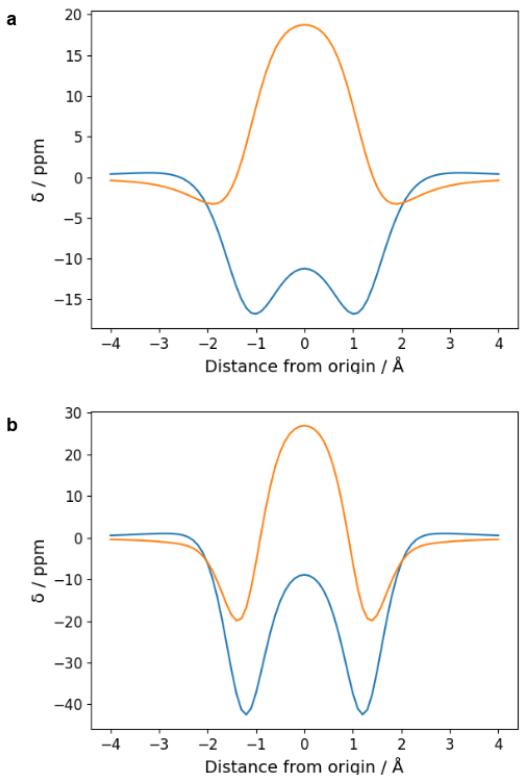

Fig. 5 Isotropically averaged chemical shift of benzene derived from 1D arrays that bisect the benzene bonds both 1 Å above the plane (**a**) and in the plane (**b**) of benzene. These are portrayed as a function of distance from the centre of the ring. The spatial location of the arrays are seen in **figure 2** with benzene. Results were obtained at the PBE0/def2-SVP level of theory.

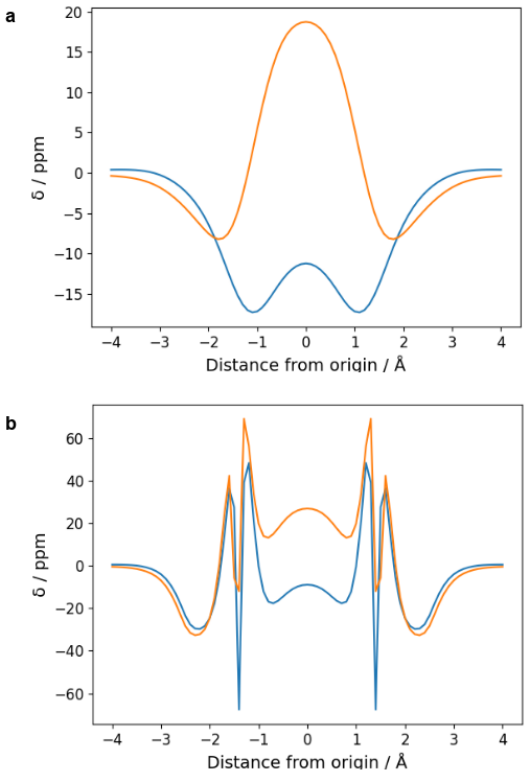

Fig. 6 Isotropically averaged chemical shift of benzene derived from 1D arrays that align with or above the benzene atoms, both 1 Å above the plane (**a**) and in the plane (**b**) of benzene. These are portrayed as a function of distance from the centre of the ring. The spatial location of the arrays are seen in **figure 2** with benzene. Results were obtained at the PBE0/def2-SVP level of theory.

and through the benzene atoms. In both of these figures, **a** represents the ghost atom array 1 Å above the plane of benzene, and **b** represents the in-plane chemical shift values. The arrays can be viewed in **figure 2**. In all of these 1D plots, *blue* lines are assigned to the S_0 state, and *orange* to the T_1 state.

Firstly, observing the NICS(1) results, we can see that the singlet plots exhibit the characteristic double-trough where the Bq array crosses the edge of benzene, and local electron density around the individual atoms causes a marginal decrease in the chemical shift. The centre of benzene has a chemical shift just under -10 ppm. This value is mimicked with the arrays placed along or above the benzene atoms, but not with the NICS(0) arrays, as expected. With the triplet states, the difference is more significant, which when taking into consideration **figure 4**, also becomes apparent.

Ultimately, whether the arrays are placed in-line with the benzene atoms, or bisecting the bonds, the absolute NICS(1) and NICS(0) values at the centre of the ring remain concordant because the atom at the centre remains the same no matter which direction the array is placed in. That being stated, the arrays that don't bisect the bonds in **figure 6** cause the graphs to become rather muddied and disrupted (especially **6b**) from the local electron densities of the benzene atoms. Therefore, coupled with NICS(1), arrays bisecting bonds like in **figure 4a**, are the least affected by these local electron densities, and should be used where possible.

Anthracene

As has been alluded to previously, anthracene is an ideal molecule to test the 2D IMS plots with, and to optimise parameters for generation of IMS plots hereafter. These results will be presented and discussed in this section.

The 4 separate NICS investigations that were performed on anthracene in different planes, resolutions, and excitation states, are depicted by **figures 7a-d**, and were obtained after geometry optimisation. **Figure 7a** represents anthracene calculated with vector spacings of 0.1 Å between the ghost atoms in the singlet state 1 Å above the plane of the molecule, and **7b** is with 0.2 Å vector spacings. There was no significant difference observed between these plots with regard to the resolution, but there was a substantial increase in the required computational time required between the two, where 493 input files were generated for **7a**, but only 126 files for **7a**, each containing 25 Bq atoms. Therefore, it was decided to generate the IMS plots hereafter using vector spacings of 0.2 Å.

Figure 7c portrays the effect of placing the Bq array in-plane with the molecule, where it becomes apparent that the σ orbital contributions are significant and grossly affect any attempt

at quantitative measurement, similarly to the in-plane NICS(1) results from benzene. Furthermore, it also makes qualitative observations more challenging, and as can be seen by comparison with **7b**, the Clar sextets are completely obscured, and one may even conclude if one were to exclusively analyse **7c**, that the terminal rings are not aromatic. This notion is clearly incorrect, as Hückel's rule predicts that with 14 π electrons, anthracene is aromatic $(4(3)+2=14)$. Additionally, anthracene is known to dimerise via a [4+4] cycloaddition reaction and undergo electrophilic substitution across the central ring, so the central ring aromaticity must be influenced by aromaticity in the terminal rings, which was originally suggested by Stanger.[17,39] Therefore, where possible, NICS(1) measurements were taken, and where not, other strategies were used to estimate IMS at 1Å above an (anti)aromatic region.

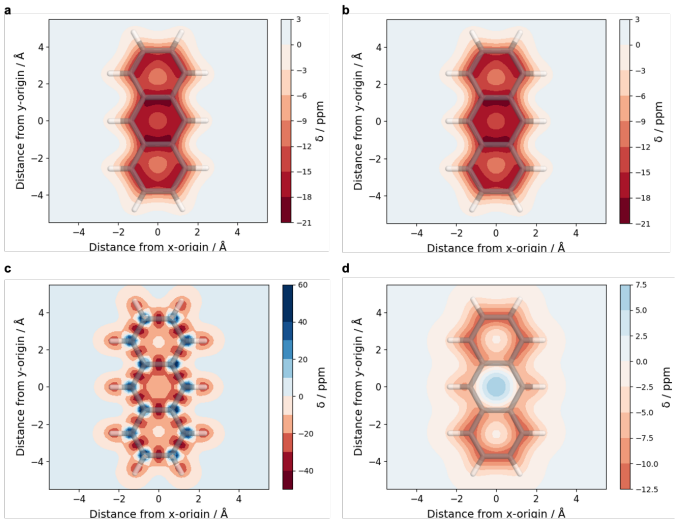

Fig. 7 Calculated IMS plots of anthracene, showing (**a**) NICS(1) singlet anthracene with 0.1 Å vector spacings, (**b**) NICS(1) singlet anthracene with 0.2 Å vector spacings, (**c**) NICS(0) singlet anthracene with 0.2 Å vector spacings, and (**d**) NICS(1) triplet anthracene with 0.2 Å vector spacings. Results were calculated at the PBE0/def2-SVP level of theory.

The final anthracene calculation, **figure 7d**, is the IMS plot of the T_1 state of anthracene. It is clear that through this method, the central anthracene ring can be observed as antiaromatic and the 2 terminal rings lose their aromaticity. NICS(1) values from the centre of either terminal ring indicate δ = (-2.5) - 0 ppm, as they are influenced by the central aromatic ring, where NICS(1) δ at the centre = 5 - 7.5 ppm. If the molecule is aromatic in the ground state, it should be antiaromatic in the triplet state according to Baird's rule, (as $4n+2$ is now indicative of antiaromaticity, whereas this would have made it aromatic in the ground state), and thus, T_1 anthracene complies with Baird's rule. Literature regarding NICS calculations of T_1 anthracene are sparse, however Baranac-Stojanović et al.[40] recently have reported that using a NICS$_{xy}$ scan, the central ring is antiaromatic, and "is somewhat delocalized onto the side rings". We don't observe quite as strong shielding effects for the central ring, and slight deshielding in the terminal rings, however largely different levels of theory have been used, as well as NICS(1) as opposed to NICS(1.7), so perhaps only rough comparisons should be drawn.

Biphenylene

Next, biphenylene was studied with the aim of demonstrating the usefulness of this method in visualising differences between antiaromatic and aromatic regions of molecules, as well as the ability for these IMS plots to distinguish differences in aromaticity between different excitation states of the same molecule, the ability of the IMS plots to visualise aromaticity in smaller ring sizes, and the accuracy of doing so by comparison to previously reported results.

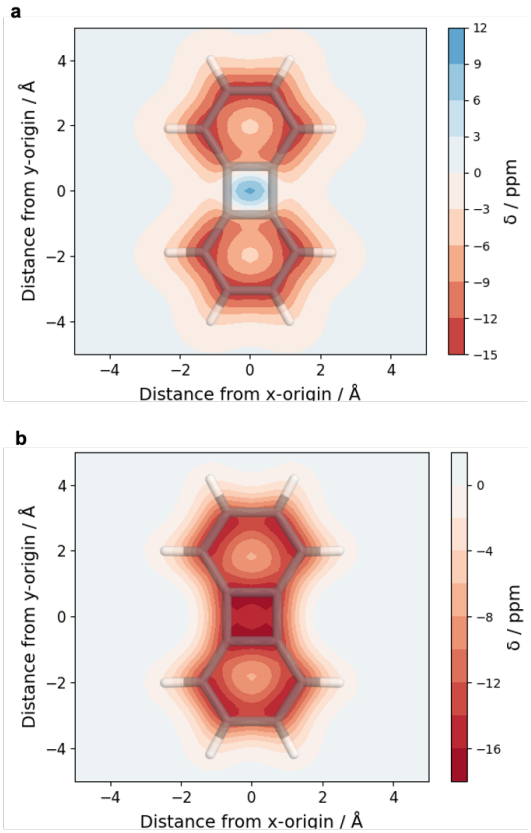

Fig. 8 IMS plots of (**a**) S_0 and (**b**) T_1 biphenylene calculated using the PBE0/def2-SVP level of theory, showing aromatic switching of biphenylene, and visual amelioration of aromatic Clar sextets in the triplet state.

Biphenylene was the second PAH tested, and is another example of a molecule which switches its aromaticity based on spin-excited states - similarly to anthracene. IMS plots are shown in **figure 8**. Unlike anthracene however, the S_0 state of biphenylene exhibits antiaromaticity in the central fused 4-membered ring, where NICS(1) δ = 9 - 12 ppm, whilst the terminal fused benzene rings are aromatic - NICS(1) δ = (-9) - (-6) ppm. Upon excitation to T_1, the central ring becomes strongly aromatic, NICS(1) δ = (-16) - (-14) ppm, but evidently, this does not significantly affect the aromaticity of the terminal rings, as NICS(1) δ at the centre of these rings is still (-8) - (-6) ppm.

To understand why, we must look at criteria for antiaromaticity and compare the S_0 to the T_1 state for resonance structures. Firstly, we will discuss triplet biphenylene from **figure 8a**. Here,

Clar sextets are clearly observed for 12π electrons which satisfies Baird's $4n$ rule for T_1 aromaticity. As this resonance form results in global aromaticity over placing all π electrons onto the terminal benzene rings, it offers greater stability. If all π orbitals are located on the terminal benzene rings for **figure 8b**, Hückel's rule is satisfied in the ground state and each of the rings have 6π electrons. However, this leaves the central ring with none, and cannot display the clear antiaromatic character it does. However, the other resonance form delocalises 2π electrons from each terminal ring onto the central one, giving the same electron configuration as cyclobutadiene, satisfying the $4n$ rule for antiaromaticity. Therefore, electrons become delocalised as characteristics from both resonance structures are observed in the final IMS plot, and the lack of clear Clar sextets in **8a** as opposed to **8b** can be comprehended.

Furthermore, these results concur with those as calculated usint the visualisation of chemical shielding tensors (VIST) method by Plasser[30], in terms of calculating regions of aromaticity and antiaromaticity.

Norcorroles

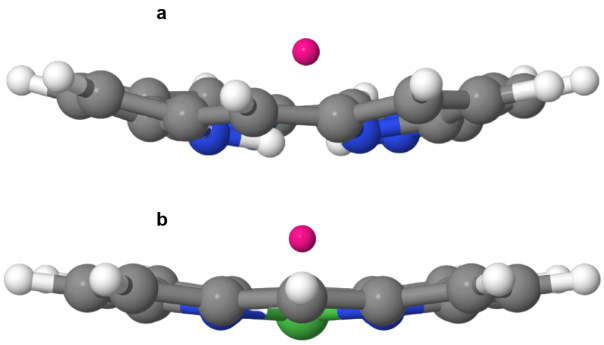

Fig. 9 A lateral view of the structures of H_2Nc (**a**), and NiNc (**b**) in JMol, after optimisation with the PBE0/def2-SVP functional and basis set, showing their bowl-shaped conformers and a single ghost atom (*pink*) where the plane of ghost atoms were added to in the centre of the macrocycle. Note that only a single Bq atom is shown and the rest have been omitted for clarity.

Next we move on to examining at larger structures and macrocycles, which exhibit more complex aromatic behaviours and nonplanarity. The first of these are norcorrole and nickel norcorrole. We are simply looking to successfully create IMS plots of these and show aromaticity and antiaromaticity from a clear perspective.

Optimisation of H_2Nc and NiNc resulted in both molecules converging to the expected structures. Lateral views of both structures can be seen in **figure 9**, which also depicts the plane the ghost atoms were added to. As can be observed, NiNc (**figure 9b**) is more planar than H_2Nc (**9a**) due to the Ni partially sterically 'locking' the macrocycle, and preventing it from having such as exaggerated a bowl shape. As mentioned previously, there is another energetically favourable conformer of H_2Nc, but for the purposes of this report, only the bowl conformer will be discussed. The structures converged as anticipated.

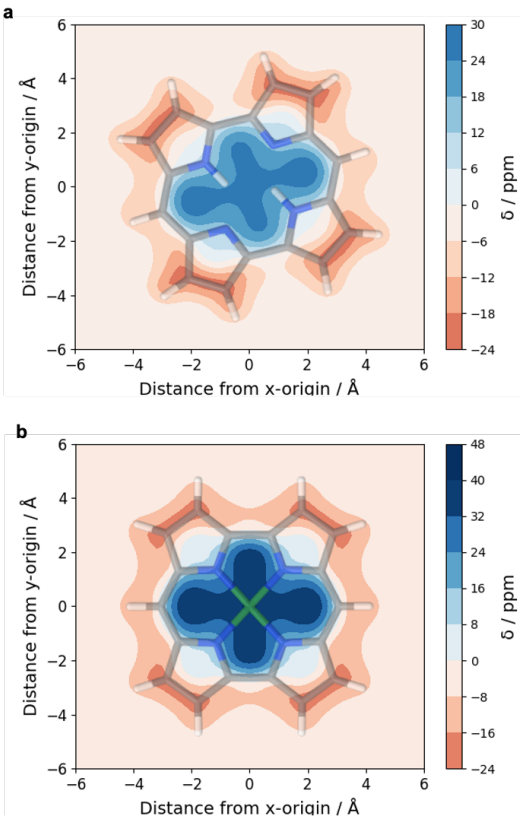

Fig. 10 IMS plots of norcorrole (**a**) and nickel norcorrole (**b**), which both exhibit aromatic and antiaromatic character. Plots were calculated with the PBE0/def2-SVP functional and basis set. See **figure 9** for more detail on where the Bq plane was placed with regard to both norcorroles.

The IMS plots in **figure 10** show a centralised antiaromatic region in the inner ring structure, with an aromatic "halo"[21] encircling the outer dipyrrin groups. In H_2Nc, the aromatic regions are apparently disturbed and broken between where the two dipyrrin structures connect, and the chemical shift rises above -6 ppm. However, in NiNc, this aromatic region remains unbroken, and the chemical shift does not rise above -8 ppm. It is impractical to attempt to quantify any NICS(1) δ at the centre of the macrocycle as is traditionally done, due to the large antiaromatic sphere at the centre of the macrocycle, and there is no merit to attempting to discuss anything other than the range of δ values observed in the aromatic region, and hence why a range has been referred to here. In both macrocycles, the 4 pyrrole-like rings are non-aromatic. These findings are in agreement with those previously reported by Karadakov.[21]

Although these IMS plots do not provide as quite a comprehensive view of norcorrole and nickel norcorrole as Karadakov's does, this technique is beneficial in that comparable results were achieved using a less computationally expensive basis set without Grimme's dispersion with Becke-Johnson damping,[41] whilst all these results have also been derived directly from Gaussian log files, rather than through the medium of Gaussian cube files. Furthermore, even if the equivalent basis set and damping were used here, performing these computations in 2D with smaller vec-

tor spacings between the Bq atoms is significantly more tractable, and perhaps even possible without the aide of HPC resources.

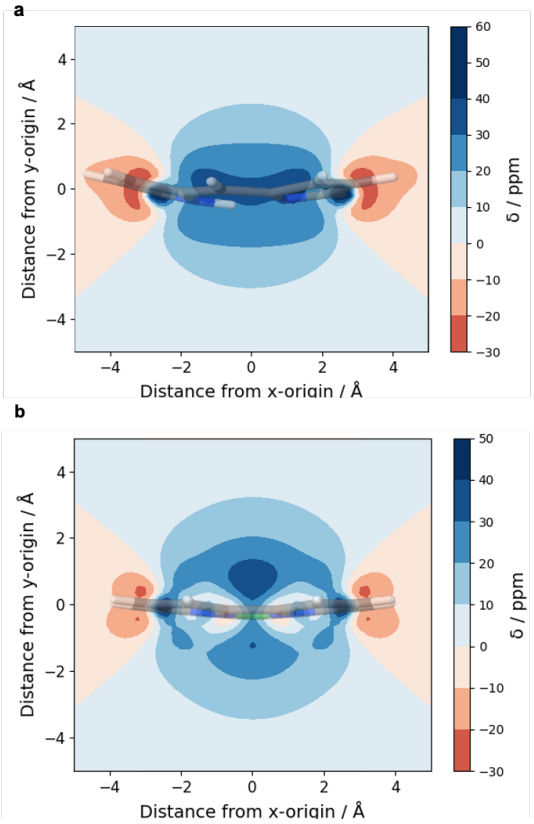

Fig. 11 Lateral views of norcorrole (**a**) and nickel norcorrole (**b**), taken through the molecules in the *yz*-plane (in relation to **figure 10**) calculated at the PBE0/def2-SVP level of theory. In the case of nickel norcorrole, this was measured +1 Å off-centre in the *x*-direction to avoid disruption from the massive electron density of the Ni atom.

More quantitative information about the structures can still be elucidated without generating large 3D plots. By bisecting the molecules with a Bq atom array in a *z*-plane, it is still possible to estimate the NICS(1) values, at specified locations, which is shown in **figure 11a**. For H_2Nc, the plane was simply placed through the centre of the system in such a way so as to avoid the non-aromatic regions. We were able to calculate chemical shifts of approximately -15 ppm 1 Å above the most aromatic region and 30 ppm for the equivalent antiaromatic region. However, this is not practical for NiNc as there is a massive contribution to chemical shift from the central Ni ion, which distorts the contours of the IMS plot by several orders of magnitude, and making determination of NICS(1) impossible. Therefore, IMS was measured as above but the Bq plane was translated 1 Å off-centre; the results of which are shown in **figure 11b**. In the Bq plane, the largest NICS(1) antiaromatic quantity measured was 40 ppm, and -20 ppm in the aromatic region. Comparison between the two molecules as to their (anti)aromatic quantities is not particularly relevant as the NICS(1) values were not measured across the same equivalent structural features.

PCT

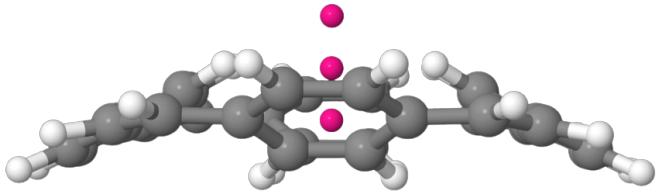

Fig. 12 A lateral view of the structure of PCT in JMol, after optimisation at the PBE0/def2-SVP level of theory, showing the different planes the Bq atoms (*pink*) were added to. From bottom to top, these are in the plane of the phenylene-connecting vinylene groups, 1 Å, and then 2 Å above this. For clarity, only a single dummy atom from each plane is shown along the central axis of the macrocycle.

Finally, the macrocycles PCT and its doubly-reduced dianion, PCT^{2-}, were studied and its alleged ability to switch between locally aromatic regions, to global aromaticity across the entire structure. According to Hückel's rule, the 32π electron PCT system should be antiaromatic, and PCT^{2-} should be aromatic (34π electrons). However Hückel's rule does not necessarily apply to macrocycles, so different methods, such as what we are investigating here, have to be used to assess aromaticity of such structures. At the time of writing, the only examples present in literature of quantitative visualisations of PCT are ACID plots used in the original paper by Eder et al.[25]; outlining PCT as a sodium ion battery electrode candidate, and VIST calculations by Plasser and Glöcklhofer.[42]

Upon optimisation of PCT, the structure converged as anticipated, with the phenylenes rotating such that they became staggered above and below the vinylene groups, as observed in **figure 12**. Unexpectedly at the time, but perhaps not so in hindsight, this was also observed with the PCT^{2-} dianion. Due to the globally aromatic nature reported for PCT^{2-}, it was anticipated to be planar. In fact, there was only a marginal difference in geometry by comparison to non-reduced PCT. Seemingly, the high steric hindrance between the hydrogens from the phenylene groups is enough to overcome the electronic effects of global delocalisation, and there is enough tolerance in the angle of the sp^2 orbitals for PCT^{2-} to remain aromatic. We can conclude here that the geometry is determined by the steric effects rather than electron conjugation. This is also observed by Plasser and Glöcklohfer in their VIST calculations of PCT and PCT^{2-}.[42] Therefore, the same approach was taken for PCT^{2-} as PCT for calculation of NICS IMS values.

In **figure 13**, 3 IMS plots of PCT are presented, and **figure 14** shows the 3 IMS plots of PCT^{2-}. In both of the figures, **a**, **b**, and **c** are Bq planes in the *xy*-direction taken at NICS(0), NICS(1), and NICS(2) respectively (relative to the vinylene groups). In **figures 13a** and **14a**, the large shielding values arising from the electron density of the atoms in close proximity to the Bq atoms are as present as ever in the vinylene linkers, however as the phenylenes are rotated relative to these, they are predominantly out-of-plane, and therefore the calculated NICS values can be effectively described, and so can their aromatic nature. In **13a**, we can clearly

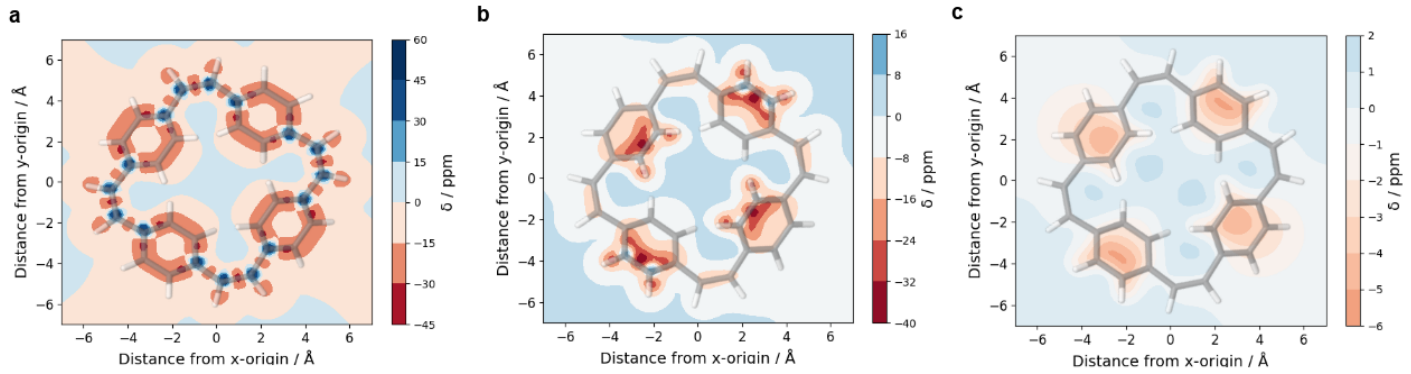

Fig. 13 IMS plots of PCT calculated with NICS(0) (**a**), NICS(1) (**b**), and NICS(2) (**c**) in relation to the plane containing the vinylene groups. In concordance with Eder et al.[25], locally aromatic regions are observed in the 4 phenylene groups, with no indication of global aromaticity throughout any of the Bq planes. Results were calculated with PBE0/def2-SVP.

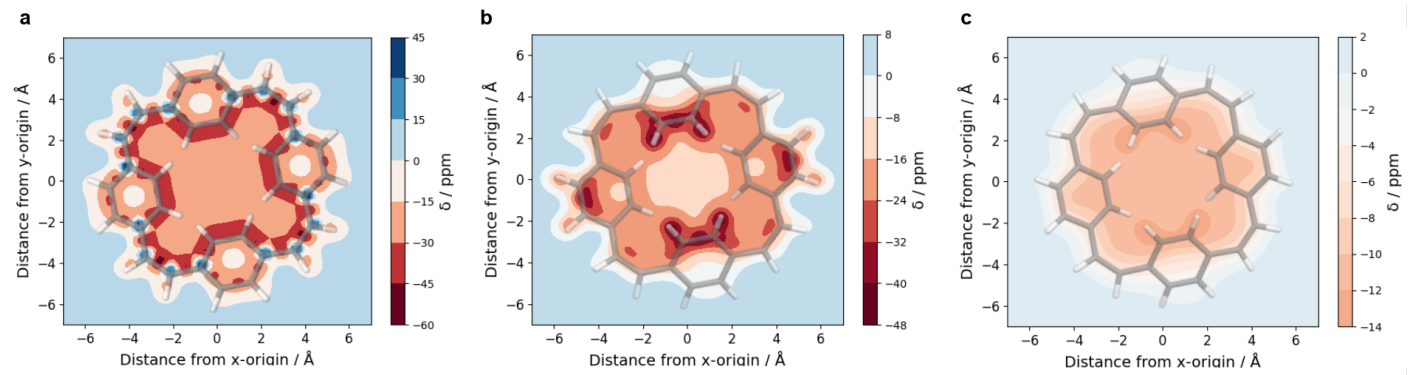

Fig. 14 IMS plots of PCT^{2-} calculated with NICS(0) (**a**), NICS(1) (**b**), and NICS(2) (**c**) in relation to the plane containing the vinylene groups. In concordance with Eder et al.[25], global aromaticity is easily intelligible for the whole structure, but we report a different conjugation pathway. Results were calculated with PBE0/def2-SVP.

observe how the individual phenylenes are aromatic, and from **13b**, NICS(1) can be approximated as $\delta \lessapprox 15$ ppm). In **14a** and **b**, the globally aromatic conjugation pathway is irrefutably present, and the specific pathway is abundantly clear. NICS(1) δ (from **figure 14b**) = (-8) - (-16) ppm for the entire macrocycle. In no instance was any antiaromatic behaviour found in PCT, debunking compliance to the $4n$ rule for prediction of antiaromaticity.

In both PCT and PCT^{2-}, **figures 13c** and **14c**, provided the clearest and least noisy qualitative image of the macrocycles, clearly showing the aromatic regions with excellent discernibility. As these plots have significantly lower chemical shift values by an approximate factor of 4, they are not particularly suitable to be commented on quantitatively.

Despite most of these results being complicit with those published by Eder et al.[25], a minor discrepancy was found. They report the conjugation pathway taken in PCT^{2-} as around the outer edges of the phenylene components of the macrocycle, however, as is represented in **figure 13a**, it shows the conjugation route as traversing the innermost portion of the phenylene rings. Evidence of this is also distinguishable in the NICS(1) plots. Whilst this may be perceived as a laborious point to make, we believe it's more suggestive of the easily misinterpretable and ambiguous nature of ACID plots, which was perspicuous when analysing the IMS-plot results.

Conclusions and Summarising Remarks

We have demonstrated the use of a new and usable method of visualising aromaticity, with the aim of making it widely accessible to the general chemistry community. We were able to successfully write python scripts to automate the addition of large arrays of ghost atoms to multiple Gaussian09 input files for the purposes of calculating NICS isotropic magnetic shielding values across entire molecules. This was achieved in both 1 and 2 dimensions, and was written with the capacity to implement 3 dimensional isosurfaces in the future. On current generally accessible computational hardware however, the 2D IMS plots should be an appropriate trade off between expense and resolution in most applications. Additionally, where needed, additional planes in the z-direction can be specified to elucidate more information, for example in non-planar structures. This is still significantly less expensive than generating full 3D isosurfaces.

We also believe to have improved upon other methods aimed at visualising aromaticity, such as the now dated ACID plots. These do not explicitly resolve structural and electronic information substantially for visualisation of complex structures and systems, and allow for easy misinterpretation. We showed this by comparing IMS plots of PCT and PCT^{2-} generated through the tool we have developed here to ACID plots of the same materials.

Whilst these results have assisted in envisaging (anti)aromatic aspects of macrocycles and other complex structures, there is still certainly a further cause for development, especially for 3D isosurface plots. Computational power still increases exponentially, as does accessibility to it, and not all facets of some larger and extremely complex structures can realistically be understood by 2D contour plots. Neither have we explored the use of CASSCF wavefunctions over DFT for dealing with strong correlation, or even substantial comparison to other functionals and basis sets.[43] CASSCF remains unfeasible for systems anywhere near this size, but would ultimately be the gold standard for visualisation of aromaticity and antiaromaticity in macrocycles.[21,44]

Acknowledgements

I wish to express my wholehearted thanks to Dr Felix Plasser for introducing me to computational and quantum chemistry, and guiding and assisting me throughout the duration of my MChem project and rest of my degree.

References

1 A. Kekulé, *Bull. Mens. la Société Chim. Paris*, 1865, **3**, 98–110.
2 E. Hückel, *Zeitschrift für Phys.*, 1931, **70**, 204–286.
3 L. Pauling and J. Sherman, *J. Chem. Phys.*, 1933, **1**, 606–617.
4 N. C. Baird, *J. Am. Chem. Soc.*, 1972, **94**, 4941–4948.
5 E. Clar, *The Aromatic Sextet*, J. Wiley, London, 1972.
6 J. Chandrasekhar, E. D. Jemmis and P. V. R. Schleyer, *Tetrahedron Lett.*, 1979, **20**, 3707–3710.
7 L. A. Paquette, W. Bauer, M. R. Sivik, M. Btihl, M. Feigel and P. V. R. Schleyer, *J. Am. Chem. Soc*, 1990, **112**, 8776–8789.
8 P. V. R. Schleyer, H. Jiao, M. N. Glukhovtsev, J. Chandrasekhar and E. Kraka, *J. Am. Chem. Soc.*, 1994, **116**, 10129–10134.
9 P. V. R. Schleyer, C. Maerker, A. Dransfeld, H. Jiao and N. J. Van Eikema Hommes, *J. Am. Chem. Soc.*, 1996, **118**, 6317–6318.
10 Z. Chen, C. S. Wannere, C. Corminboeuf, R. Puchta and P. V. R. Schleyer, *Chem. Rev.*, 2005, **105**, 3842–3888.
11 D. Sundholm, H. Fliegl and R. J. Berger, *Wiley Interdiscip. Rev. Comput. Mol. Sci.*, 2016, **6**, 639–678.
12 M. J. Frisch, G. W. Trucks, H. B. Schlegel, G. E. Scuseria, M. A. Robb, J. R. Cheeseman, G. Scalmani, V. Barone, B. Mennucci, G. A. Petersson, H. Nakatsuji, M. Caricato, X. Li, H. P. Hratchian, A. F. Izmaylov, J. Bloino, G. Zheng, J. L. Sonnenberg, M. Hada, M. Ehara, K. Toyota, R. Fukuda, J. Hasegawa, M. Ishida, T. Nakajima, Y. Honda, O. Kitao, H. Nakai, T. Vreven, J. A. Montgomery, Jr., J. E. Peralta, F. Ogliaro, M. Bearpark, J. J. Heyd, E. Brothers, K. N. Kudin, V. N. Staroverov, R. Kobayashi, J. Normand, K. Raghavachari, A. Rendell, J. C. Burant, S. S. Iyengar, J. Tomasi, M. Cossi, N. Rega, J. M. Millam, M. Klene, J. E. Knox, J. B. Cross, V. Bakken, C. Adamo, J. Jaramillo, R. Gomperts, R. E. Stratmann, O. Yazyev, A. J. Austin, R. Cammi, C. Pomelli, J. W. Ochterski, R. L. Martin, K. Morokuma, V. G. Zakrzewski, G. A. Voth, P. Salvador, J. J. Dannenberg, S. Dapprich, A. D. Daniels, O. Farkas, J. B. Foresman, J. V. Ortiz, J. Cioslowski and D. J. Fox, *Gaussian09 Revision E.01*, Gaussian Inc. Wallingford CT 2009.
13 *Molecule Specifications | Gaussian.com*, https://gaussian.com/molspec/.
14 P. V. R. Schleyer, H. Jiao, N. J. R. v. E. Hommes, V. G. Malkin and O. L. Malkina, *J. Am. Chem. Soc.*, 1997, **119**, 12669–12670.
15 P. V. R. Schleyer, B. Kiran, D. V. Simion and T. S. Sorensen, *J. Am. Chem. Soc.*, 2000, **122**, 510–513.
16 P. V. R. Schleyer, M. Manoharan, H. Jiao and F. Stahl, *ACS Org. Lett.*, 2001, **3**, 3643–3646.
17 A. Stanger, *J. Org. Chem.*, 2006, **71**, 883–893.
18 P. B. Karadakov, P. Hearnshaw and K. E. Horner, *J. Org. Chem.*, 2016, **81**, 11346–11352.
19 B. J. Lampkin, Y. H. Nguyen, P. B. Karadakov and B. Vanveller, *Phys. Chem. Chem. Phys.*, 2019, **21**, 11608–11614.
20 B. J. Lampkin, P. B. Karadakov and B. VanVeller, *Angew. Chemie Int. Ed.*, 2020, **59**, 19275–19281.
21 P. B. Karadakov, *ACS Org. Lett.*, 2020, **22**, 8676–8680.
22 A. Ghosh, I. H. Wasbotten, W. Davis and J. C. Swarts, *Eur. J. Inorg. Chem.*, 2005, **2005**, 4479–4485.
23 T. Ito, Y. Hayashi, S. Shimizu, J. Y. Shin, N. Kobayashi and H. Shinokubo, *Angew. Chemie - Int. Ed.*, 2012, **51**, 8542–8545.
24 J. Conradie, C. Foroutan-Nejad and A. Ghosh, *Sci. Rep.*, 2019, **9**, 4852.
25 S. Eder, D. Yoo, W. Nogala, M. Pletzer, A. Santana Bonilla, A. J. P. White, K. E. Jelfs, M. Heeney, J. W. Choi and F. Glöcklhofer, *Angew. Chemie Int. Ed.*, 2020, **59**, 12958–12964.
26 D. Morgan and F. Plasser, *ims-plot: a tool for multidimensional visualisation of aromaticity in macrocycles*, https://github.com/dylanbmorgan/ims-plot.git.
27 *Jmol: an open-source Java viewer for chemical structures in 3D*, http://www.jmol.org/.
28 *The Open Babel Package, version 2.4.2*, http://openbabel.org/.
29 *NMR | Gaussian.com*, https://gaussian.com/nmr/.
30 F. Plasser, *MDPI Chem.*, 2021, **3**, 532–549.
31 J. P. Perdew, K. Burke and M. Ernzerhof, *Phys. Rev. Lett.*, 1996, **77**, 3865–3868.
32 J. P. Perdew, K. Burke and M. Ernzerhof, *Phys. Rev. Lett.*, 1997, **78**, 1396.
33 M. Ernzerhof and G. E. Scuseria, *J. Chem. Phys.*, 1999, **110**, 5029–5036.
34 C. Adamo and V. Barone, *J. Chem. Phys.*, 1999, **110**, 6158–6170.
35 A. Schäfer, H. Horn and R. Ahlrichs, *J. Chem. Phys.*, 1992, **97**, 2571–2577.
36 A. Schäfer, C. Huber and R. Ahlrichs, *J. Chem. Phys.*, 1994, **100**, 5829–5835.
37 F. Weigend and R. Ahlrichs, *Phys. Chem. Chem. Phys.*, 2005, **7**, 3297–3305.
38 F. Weigend, *Phys. Chem. Chem. Phys.*, 2006, **8**, 1057–1065.
39 G. W. Breton and X. Vang, *J. Chem. Educ.*, 1998, **75**, 81.
40 M. Baranac-Stojanović, M. Stojanović and J. Aleksić, *New J.*

Chem., 2021, **45**, 5060–5074.

41 S. Grimme, S. Ehrlich and L. Goerigk, *J. Comput. Chem.*, 2011, **32**, 1456–1465.

42 F. Plasser and F. Glöcklhofer, *European J. Org. Chem.*, 2021, **2021**, 2529–2539.

43 B. O. Roos, P. R. Taylor and P. E. M. Sigbahn, *Chem. Phys.*, 1980, **48**, 157–173.

44 D. S. Levine, D. Hait, N. M. Tubman, S. Lehtola, K. B. Whaley and M. Head-Gordon, *J. Chem. Theory Comput.*, 2020, **16**, 2340–2354.